A Chromatic-Aberration Diagnostic Based on a Spectrally Resolved Lateral-Shearing Interferometer

Spatiotemporal coupling in an ultrashort-pulse beam is an important feature that must be characterized for laser–matter interactions and focal-spot improvement. Pulse-front tilt (PFT) arising from a misaligned compressor-grating pair or a simple prism disperses the spatial and spectral envelope of the pulse at focus with respect to wavelength, thereby lowering the available peak power density.[1] Radial-group delay (RGD) arising in a circularly symmetric, refractive-image relay similarly smears the focal spot transversely and longitudinally.[2] Compensation schemes for PFT and RGD based on diffraction and refraction were proposed in Refs. 3 and 4. Space–time coupling can be beneficial in some experimental configurations. Spatial chirp in the beam obtains maximum spatial and spectral overlap at focus, creating a "temporal-focusing effect," which has been useful in the area of micromachining[5] and microscopy.[6] The wavefront-rotation effect introduced by focusing a pulse with PFT creates an angularly separated burst of attosecond pulses reflecting off the laser-induced plasma.[7]

A diagnostic is needed to compensate for and control the spatiotemporal effects, not only from well-defined optical systems but also from nonuniform optical properties such as in dielectric optical coatings. A second-harmonic, single-shot autocorrelator can be used to measure the pulse-front tilt angle[8] or the effect of pulse broadening caused by RGD.[9] Linear autocorrelation methods infer the angle or the curvature of the pulse-front delay by examining, in multiple steps, the fringes between two beams.[2] Other linear techniques are based on spectrally resolving spatial interference. These methods analyze the spectrum of the interference between two laterally sheared fields of the same test beam[10] or between the test and reference fields,[11] where the carrier terms are introduced by either temporal delay or relative tilt; direct fringe analysis can be employed for certain referenced schemes.[12] All these spectral interference methods require a separate system of beam splitters and combiners external to the spectrometer. Scanning the spectral interferogram with a fiber tip[13] or using phase diversity on a cylindrically symmetric beam[14]—both require multiple measurement steps and have been demonstrated. A rather unique scheme called STRIPED FISH[15] provides discrete samples of spectral slices with full two-dimensional (2-D) intensity and phase mapping at each slice by interfering each slice with a reference beam; however, spatial and spectral resolution of this method is poor.

A simpler, spectrally resolved lateral-shearing interferometer is proposed in this work. The separate preconditioning system introducing delay or tilt is replaced by a single Ronchi grating located in front of the entrance slit of a spectrometer. No moving parts are involved; therefore, calibration is performed only once. Full one-dimensional (1-D) chromatic aberrations can be characterized in a single-shot measurement.

The side and top views of the setup are schematically shown in Fig. 145.54, with the spectrometer system laid out linearly.
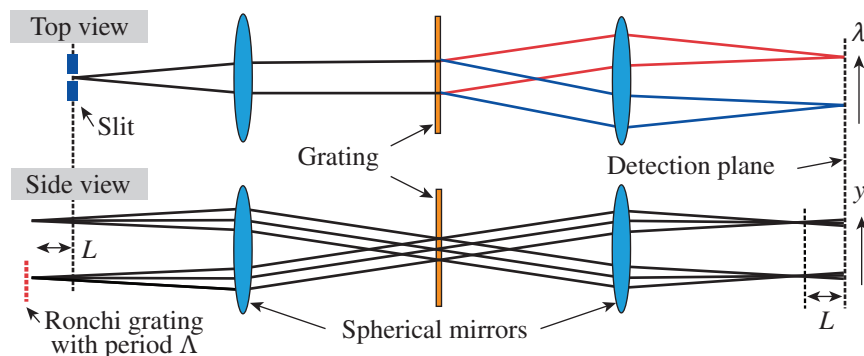

Figure 145.54
A schematic of a spectrally resolved lateral-shearing interferometer. The entrance slit is spectrally resolved in a tangential plane, whereas the sagittal image of the slit is interfered to create a sheared interferogram from which spatial phase can be extracted. Only zeroth- and first-order diffractions are shown in the side view. For convenience, the rays reflected by the spherical mirrors and the spectrometer grating are shown on the other side of the mirror as if they are passing through.

The top view representing the beam diffracting in the horizontal plane corresponds to a normal spectrometer system. The side view shows the beam diffracting through the Ronchi grating in the vertical plane. The detector images the spectrometer slit. The Ronchi plane is imaged before the detector plane; therefore, the first-order diffraction beams are sheared at the detector plane. If the beam is sampled at a fixed horizontal coordinate x_0 by the spectrometer slit, the field at the detector plane going through a Ronchi grating of periodicity Λ is represented by[16]

$$E(x_0, y, \omega) = \sum_{m=0,\pm 1,\dots} \eta_m A\left(x_0, y + m\frac{2\pi c L}{\omega \Lambda}\right)$$

$$\times \exp\left(i\frac{2\pi m}{\Lambda}y + i|m|\omega\tau\right), \qquad (1)$$

where $A(x_0, y, \omega)$ is the spectral envelope and phase at position y at the entrance slit. The index m is the diffraction order and η_m is the diffraction efficiency at the mth order. The spatial coordinate x_0, hereafter, will not be shown. L is the distance from the Ronchi grating to the entrance slit and τ is the arrival time difference between the first- and zeroth-order diffraction beams; τ is sufficiently small that spectral fringes are not observed. The 1-D Fourier-domain analysis of the interferogram along the spatial axis can separate out the first harmonic H_1 (i.e., the interaction between fields at $m = 0$ and $m = \pm 1$) from dc and higher-order terms. With the phase of $A(y, \omega)$ defined as $\varphi(y, \omega)$, the first harmonic is

$$H_1 \sim |A(y, \omega)|^2 \exp\left(i\frac{2\pi c L}{\omega \Lambda}\frac{\partial \varphi}{\partial y}\right)\cos(\omega\tau)\exp\left(i\frac{2\pi}{\Lambda}y\right). \qquad (2)$$

The phase of H_1, except for the carrier term, contains a phase derivative from which spectrally coupled 1-D spatial phase can be integrated. Purely spectral phase without spatial dependence cancels out in the derivative so it is not measurable in this approach.

Pulse-front delay (PFD) and RGD are linear and quadratic-phase components whose magnitudes vary linearly with the spectral deviation. The phase can be decomposed into chromatic and achromatic components, denoted as $g(y)$ and $f(y)$, respectively:

$$\varphi(y, \omega) = (\omega - \omega_0)\,g(y) + \frac{\omega}{c}\,f(y), \qquad (3)$$

where $f(y)$ is an optical-path difference function in units of distance and $g(y)$ is a relative group delay in units of time; $f(y)$ can be represented as

$$f(y) = \theta_y\,y + y^2/(2R_y) + f_{HO}(y), \qquad (4)$$

where θ_y and R_y are the tilt and radius of curvature in the y dimension, respectively, and $f_{HO}(y)$ is the remaining higher-order term. Likewise, $g(y)$ is the sum of linear, quadratic, and higher-order terms $[g_{HO}(y)]$:

$$g(y) = \alpha\left(\frac{y}{r}\right) + \beta\left(\frac{y}{r}\right)^2 + g_{HO}(y), \qquad (5)$$

where r is the radius of the beam and $\alpha = \mathrm{PFD}(r) - \mathrm{PFD}(0)$ and $\beta = \mathrm{RGD}(r) - \mathrm{RGD}(0)$. Equations (3) and (5) suggest that the PFD shifts the carrier-phase offset linearly with respect to frequency change, and RGD modifies the carrier frequency linearly with respect to frequency change. The fringe patterns with PFD or RGD dominant cases are illustrated in Fig. 145.55.
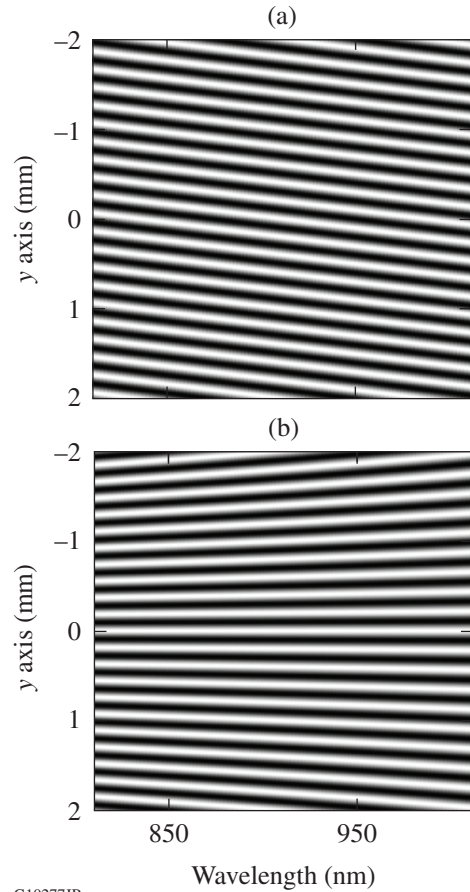
G10277JR

Figure 145.55
Examples of fringe patterns. (a) The tilted fringe indicates pulse-front tilt and (b) the fanning-out fringe indicates radial-group delay.

The algebraic form of $(2\pi cL)/(\omega\Lambda) \cdot \partial\varphi/\partial y$, consistent with Eqs. (3)–(5), is

$$\frac{2\pi cL}{\omega\Lambda}\frac{\partial\varphi}{\partial y} \triangleq \Delta\varphi = c_1 + c_2 y + (c_3 + c_4 y)(\lambda - \lambda_0). \quad (6)$$

Comparing Eqs. (4) and (5), the coefficients of Eq. (6) are determined as

$$c_1 = 2\pi\frac{L}{\Lambda}\theta_y, \quad (7)$$

$$c_2 = 2\pi\frac{L}{R_y\Lambda}, \quad (8)$$

$$c_3 = -\frac{2\pi c}{\lambda_0}\frac{L\alpha}{\Lambda r}, \quad (9)$$

$$c_4 = -\frac{4\pi c}{\lambda_0}\frac{L\beta}{\Lambda r^2}. \quad (10)$$

Extracting RGD and PFD information directly from the low-order polynomial fit of $\Delta\varphi$ is less ambiguous than fitting Eq. (3) to the numerically integrated data of $\Delta\varphi$ because of the arbitrary integration constant.

A test bed was set up to measure RGD in a simple refractive system, as shown in Fig. 145.56. The broadband source is a spectrally incoherent, superluminescent light-emitting diode (SLED) with spectral density from 968 to 1076 nm. An actual ultrashort pulse was not required for the demonstration because only relative phases are required to characterize space–time coupling. The SLED is coupled to a single-mode fiber whose tip is used as a point source. A 200-mm-focal-length concave mirror collimates the diverging beam from the fiber tip. The off-axis configuration of the concave mirror introduces astigmatism, but it is not important since the wavefront must be collimated only in the sagittal plane parallel to the spectrometer

slit. The collimated beam is sent to the test telescope (L3 and L4) through a 5-mm input aperture. The aperture plane is imaged to M2 and to the slit. The imaging requirement minimizes the chromatic effect on the beam size. The focal lengths of L3 and L4 are 71.6 mm (fused silica) and 378.9 mm (BK7) at 1037 nm, respectively. The calculated RGD of the test telescope in a double-pass configuration is 50.6 fs over a 5-mm aperture. The input aperture is re-imaged through the beam splitter (BS) to the spectrometer slit by an imaging telescope (L1, L2). L1 and L2 have the same 61.0-mm focal length. The single-pass RGD in the imaging telescope is 0.9 fs over 5 mm. The spectrometer is a Czerny–Turner type with a grating groove density of 150 lines/mm (SP-2556, Princeton Instruments). The chromatic aberrations in the imaging telescope are calibrated using a reference interferogram by inserting a retroreflective mirror (M1) behind the aperture. The reference phase is always subtracted from the measured phase.

The distance between the spherical mirrors is shorter than $2f$, so the collimated input beam slightly diverges at the detector plane in the side view. This is because the commercial spectrometer is required to image only the horizontal dimension while keeping its size compact. The beam sizes at the entrance slit and at the detector plane are, however, the same. The period of the Ronchi grating is separately calibrated using an independently collimated source. The period is found to be 201.1 μm by analyzing the projected image of the Ronchi grating in the Fourier domain.

The measured interferogram and the reconstructed phase are shown in Fig. 145.57. The fringe spacing in Fig. 145.57(a) increases slightly from left to right, indicating the presence of RGD. The reconstructed phase in Fig. 145.57(b) shows the wavelength-dependent quadratic phase, where the curves are spaced out by arbitrary integration constants for visualization purposes. The top curve corresponds to 1068 nm and the bottom to 970 nm. The distance from the Ronchi to the slit, L, is 30.08 mm. To maximize the fringe contrast, L is approximately set to a multiple of the Talbot distance. The measured RGD is
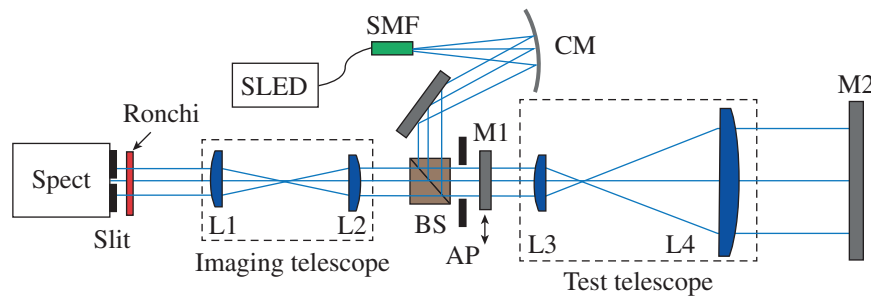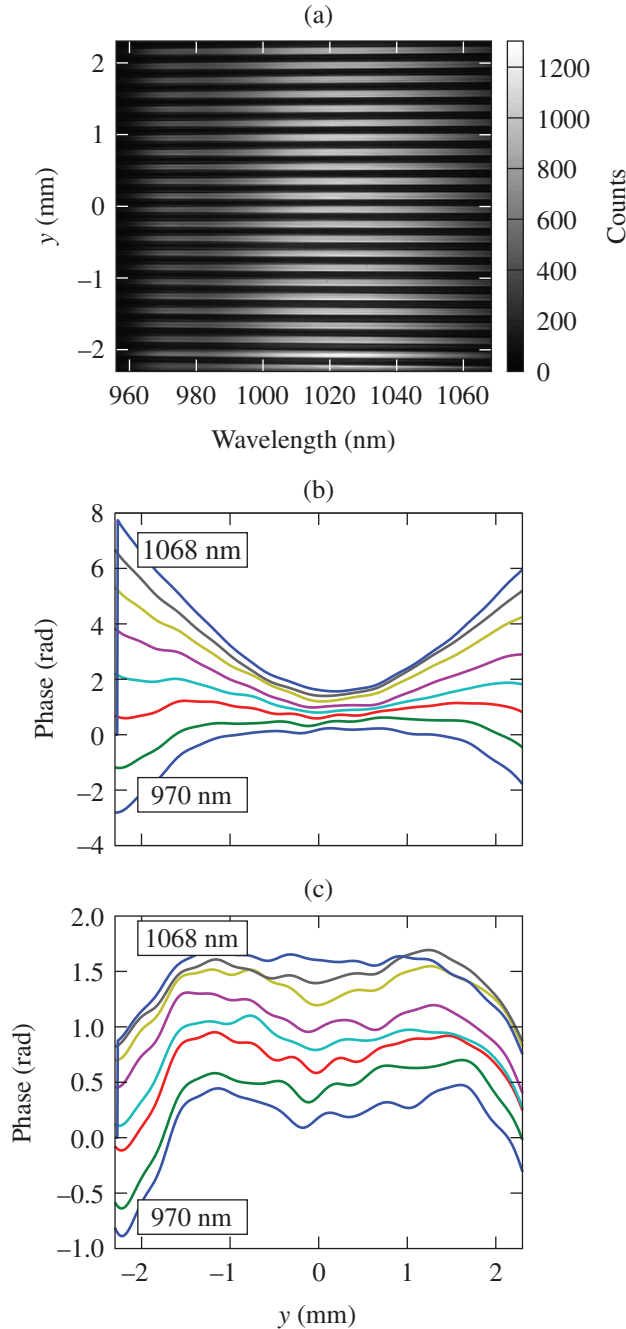

Figure 145.56
Experimental setup. SLED: superluminescent light-emitting diode; SMF: single-mode fiber; CM: concave mirror; BS: beam splitter; AP: aperture; M1 and M2: mirrors; L1–L4: lenses; Spect: spectrometer.
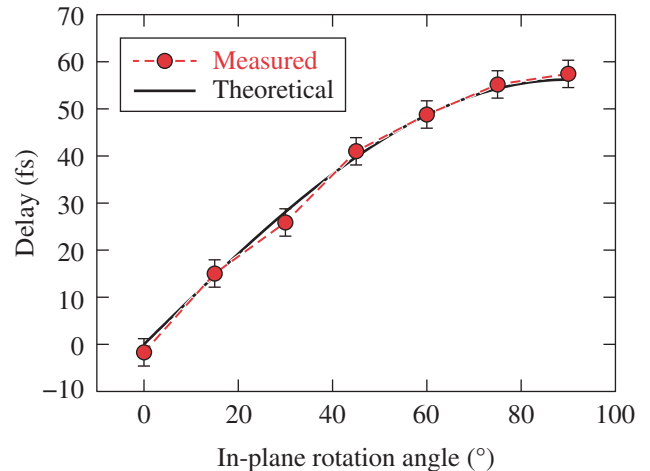
E24766JR

51.1 fs using Eq. (10), which is within 1% of the direct calculation based on dispersion and lens curvature.[17] Figure 145.57(c) shows the sum of both chromatic and achromatic higher-order terms, which is mainly the spherical aberration (i.e., fourth-order phase) in the system.

A PFD measurement was demonstrated using a BK7 prism (wedge angle of 11°20′) mounted on a rotation stage and placed in front of the Ronchi grating. Since PFD is measured only in the vertical direction (y axis) in this setup, the PFD along the y axis can be varied according to the in-plane rotation angle. Because of the beam deviation and pointing error on insertion of the wedge, the beam centering and pointing must be restored. A flipper mirror was installed between the wedge and the Ronchi grating to send the beam to the pointing and centering diagnostic cameras. The two mirrors between the wedge and L1 were adjusted to restore the alignment. The beam position was aligned within ±50 μm and the pointing within ±150 μrad, with respect to the reference positions recorded without the wedge. The rather large pointing inaccuracy comes mainly from the mechanical instability of the flipper mirror. The simulation suggests this level of fluctuation introduces only a ±0.5-fs error in PFD. The centering camera images the beam at the equivalent imaging plane of the spectrometer slit. The exact centering alignment becomes important in proportion to the amount of RGD, because any centering shift mixed with RGD [i.e., c_4 of Eq. (10)] will result in additional c_3 as calculated by Eq. (9), which is used to estimate PFD. The insertion of retro-mirror M1 redirects the beam through only the imaging telescope (L1 and L2). The aperture diameter was set to 6 mm. The relative PFD with the wedge is shown in Fig. 145.58. The PFD as measured at seven different angles shows good agreement compared with the calculated PFD. The error bar is the standard deviation of the measured fluctuation in five independent sets of measurements. The PFD at 90° rotation

E24767JR

Figure 145.57
Experimental results. (a) Interferogram image, (b) the lineouts of the reconstructed phase at different wavelengths, and (c) the higher-order phase.

E24768JR

Figure 145.58
Experimental results of measuring the variable pulse-front tilt using an 11° prism.

(wedge parallel to the slit) is 56.2 fs. The standard deviation of the measured PFD with respect to theoretical values is 1.4 fs.

Both RGD and PFD are dependent on beam size; an exact beam size must be specified for given RGD and PFD values. The angle of pulse-front tilt ($\theta_{\Delta T}$) and the temporal radius of curvature in the radial-group delay ($R_{\Delta T}$) could be useful alternatives that are independent of beam size. From the definition of group delay ($\partial\varphi/\partial\omega$), $\theta_{\Delta T}$ is found to be $c\alpha/r$ and $R_{\Delta T}$ is $r^2/(2\beta c^2)$; $R_{\Delta T}$ is 682 ps in the above experiment.

A slightly different arrangement of the system could provide greater flexibility. The Ronchi grating, for example, can be placed directly in front of the detector rather than in front of the entrance slit. Additionally, the input beam rotated by 90° can provide the PFD and RGD information in the orthogonal direction. The rotated beam can also be stacked on top of the original beam to provide 2-D information in a single shot.

The form of Eqs. (6), (9), and (10) suggests that the absolute calibration of the wavelength axis is not necessary for estimating chromatic aberrations (i.e., PFD and RGD) as long as the center wavelength λ_0 is known. The error in the estimation of the absolute wavelength will result in the estimation of the achromatic term [$f(y)$ in Eq. (3)] but not in the chromatic terms. A compact setup made of a non-imaging, dispersive element and a Ronchi or a similar grating might be able to provide the same information.

Regarding the measurements of low-order chromatic aberrations, the full spectrum may not be required. A combination of separate measurements using only narrow-bandwidth sources can also provide the RGD. Reprocessing the data using 2-nm-bandwidth, numerically cropped segments of the measured interferogram at three points (970 nm, 1000 nm and 1030 nm) still results in an RGD within a 1% error. The effect of noise between separate measurements, however, has not yet been evaluated.

A simple, spectrally resolved, 1-D lateral-shearing interferometer that can be used to characterize spatiotemporal coupling in a single shot has been demonstrated. The setup requires only a single Ronchi grating attached in front of a spectrometer. The calibration is done only once, and it can be easily transported. Its accuracy was experimentally demonstrated in the measurements of RGD and PFD. Suggestions have been made on different ways of implementing the basic idea and on the possibility of improving and simplifying the system.

REFERENCES

1. G. Pretzler, A. Kasper, and K. J. Witte, Appl. Phys. B **70**, 1 (2000).

2. H.-M. Heuck *et al.*, Appl. Phys. B **84**, 421 (2006).

3. J. Néauport, Appl. Opt. **46**, 1568 (2007).

4. S.-W. Bahk, J. Bromage, and J. D. Zuegel, Opt. Lett. **39**, 1081 (2014).

5. D. N. Vitek *et al.*, Opt. Express **18**, 18,086 (2010).

6. G. Zhu *et al.*, Opt. Express **13**, 2153 (2005).

7. H. Vincenti and F. Quéré, Phys. Rev. Lett. **108**, 113904 (2012).

8. Z. Sacks, G. Mourou, and R. Danielius, Opt. Lett. **26**, 462 (2001).

9. T. A. Planchon *et al.*, Opt. Lett. **29**, 2300 (2004).

10. C. Dorrer and I. A. Walmsley, Opt. Lett. **27**, 1947 (2002).

11. J. Jasapara and W. Rudolph, Opt. Lett. **24**, 777 (1999).

12. A. P. Kovács *et al.*, Appl. Phys. B **80**, 165 (2005).

13. P. Bowlan *et al.*, Opt. Express **14**, 11,892 (2006).

14. P. Bowlan and R. Trebino, J. Opt. Soc. Am. B **29**, 244 (2012).

15. P. Gabolde and R. Trebino, Opt. Express **14**, 11,460 (2006).

16. J. Primot and N. Guérineau, Appl. Opt. **39**, 5715 (2000).

17. Z. Bor, J. Mod. Opt. **35**, 1907 (1988).